ACCSCIENCE PUBLISHING

International Journal of Bioprinting

RESEARCH ARTICLE

# Thermally tunable and biodegradable copolymer ink for 3D-printed implantable drug delivery depots

**Yun Geun Jeong[1†], Joon Yeong Park[1†], Moon Hee Lim[1], James J. Yoo[2], Sang Jin Lee[2], and Moon Suk Kim[1,3*]**

[1]Department of Molecular Science and Technology, Ajou University, Suwon, Gyeonggi, South Korea

[2]Wake Forest Institute for Regenerative Medicine, Wake Forest School of Medicine, Winston-Salem, North Carolina, United States of America

[3]Research Institute, Medipolymer, Suwon, Gyeonggi, South Korea

## Abstract

Three-dimensional (3D) printing enables precise, patient-tailored drug delivery, but its broader potential is limited by the lack of polymers that combine low processing temperatures with tunable biodegradability. This study presents the rational design, synthesis, and characterization of poly(ε-caprolactone-ran-lactide) (CL) polymer inks with tunable printability and controllable biodegradability for 3D-printed implantable drug delivery applications. By varying the poly(lactide) (PLA) content (1–20 mol%) within the poly(ε-caprolactone) backbone, the thermal and mechanical properties of the CL copolymers were precisely adjusted to meet both printing and biological performance criteria. Differential scanning calorimetry revealed that increasing PLA content systematically reduced the melting temperature (from 57 to 40°C), enabling thermal modulation of printability and depot shape retention. Rheological and printability assessments, conducted under optimized chamber temperature, feed rate, and extrusion pressure, demonstrated excellent filament continuity, layer stacking fidelity, and shape preservation. Among the synthesized variants, CL1–CL3 maintained structural stability above 40°C and were selected for detailed evaluation. The polymer inks were further validated through the fabrication of dexamethasone (Dex)-loaded CL (Dex-CL) depots, which achieved high encapsulation efficiency (>90%) and exhibited sustained drug release over 30 days in both *in vitro* and *in vivo* models. Notably, the lower melting point of Dex-CL3 contributed to accelerated release kinetics, confirming the utility of PLA content as a tunable parameter for degradation control. *In vivo* studies demonstrated prolonged Dex retention with minimal local inflammation, as confirmed by histological analysis. The CL polymer inks showed excellent biocompatibility and tissue integration, underscoring their potential for biomedical implantation. Collectively, these findings demonstrate that CL polymer inks provide a robust platform for 3D printing implantable drug depots with customizable degradation profiles, reliable structural performance, and immunological safety, supporting their use in sustained and responsive therapeutic delivery systems.

***Keywords:*** 3D printing; Biocompatibility; Biodegradability; Drug delivery; Polymer inks; Printability

†These authors contributed equally to this work.

***Corresponding author:**
Moon Suk Kim
(moonskim@ajou.ac.kr)

**Citation:** Jeong YG, Park JY, Lim MH, Yoo JJ, Lee SJ, Kim MS. Thermally tunable and biodegradable copolymer ink for 3D-printed implantable drug delivery depots. *Int J Bioprint*. 2025;11(5):350-370. doi: 10.36922/IJB025290294

**Received:** July 18, 2025
**1st revised:** August 22, 2025
**2nd revised:** August 25, 2025
**Accepted:** August 26, 2025
**Published online:** August 26, 2025

## 1. Introduction

Drug delivery systems (DDS) are essential in modern medicine, enabling targeted, sustained, and controlled release of therapeutic agents while minimizing systemic side effects. Traditional DDS platforms, including tablets, microparticles, and hydrogels, have enabled varying degrees of temporal control over drug release.[1,2] However, these systems often fall short in terms of spatial targeting, consistent release kinetics, and adaptability to patient-specific needs. To address these limitations, three-dimensional (3D) printing has recently garnered increasing attention as a powerful tool for next-generation DDS, enabling precise spatial and temporal control over drug release and the fabrication of patient-tailored geometries.[3,4]

Among various 3D printing methods, semi-solid extrusion prints viscoelastic pastes or gels at ambient or moderately elevated temperatures, thereby minimizing thermal degradation and better preserving heat-sensitive components. However, it often necessitates solvent removal or post-printing crosslinking, which may reduce microarchitectural precision and introduce residual solvents. By contrast, fused deposition modeling (FDM) is particularly well suited for DDS applications because it provides simplicity, cost-effectiveness, and high reproducibility in producing multilayered drug delivery architectures.[5–7] Nevertheless, FDM requires polymer melting above the softening point, which can compromise the stability of thermolabile drugs or materials with narrow processing windows.

Thus, while FDM enables precise, solvent-free fabrication, its reliance on high processing temperatures remains a critical limitation. Addressing this challenge requires the development of polymer formulations with sufficiently low melting points ($T_m$), yet adequate mechanical strength, degradability, and biocompatibility.[8]

Biodegradable aliphatic polyesters, such as poly(ε-caprolactone) (PCL) and poly(lactide) (PLA), are among the most widely studied materials for 3D-printed DDS.[9] PCL is known for its excellent biocompatibility, flexibility, and relatively low $T_m$ (~60°C), making it well-suited for low-temperature printing.[10,11] However, its slow degradation rate significantly limits its utility in applications requiring controlled or timely drug release.[12,13] In contrast, PLA degrades more rapidly but has a high $T_m$ (~175°C), restricting its use in thermally sensitive FDM processes.[14]

Random copolymerization of PCL and PLA to form poly(ε-caprolactone-ran-lactide) (CL) offers a promising strategy to overcome these individual drawbacks, allowing the development of materials with tunable thermal, mechanical, and degradation properties. By adjusting the PLA content within the PCL matrix, both the $T_m$ and biodegradation rate can be modulated simultaneously, enabling CL polymer inks optimized for printability and therapeutic performance.[15,16] Such customized formulations not only offer the potential for precise drug release profiles but also enhanced structural fidelity during FDM printing.[17–20]

In this study, dexamethasone (Dex)—a corticosteroid widely applied for anti-inflammatory treatment—was selected as the model drug owing to its well-established anti-inflammatory efficacy, extensive use in preclinical DDS evaluations, and compatibility with both *in vitro* and *in vivo* assays.[21] Although Dex possesses high thermal stability (reportedly up to ~200°C) and can be processed using high-melting polymers such as PLA, our primary objective was to demonstrate the feasibility, long-term stability, and sustained-release performance of the CL-based implantable DDS platform under clinically relevant conditions. Given that our DDS is intended for long-term, localized delivery, Dex was chosen for its proven stability over extended implantation periods and its therapeutic relevance in chronic inflammatory disorders. To validate their utility as drug delivery vehicles, Dex was incorporated into the CL polymer inks and formulated into Dex-loaded CL (Dex-CL) depots. These depots were comprehensively evaluated through *in vitro* and *in vivo* studies to examine drug release kinetics and inflammatory response. Collectively, these analyses establish the CL polymer inks as a versatile platform for 3D-printed implantable drug depots. This work demonstrates the rational design of CL polymer inks with tunable printability and degradability, offering promising potential for advanced, sustained-release therapeutic systems.

## 2. Materials and methods

### 2.1. Materials

Methoxy poly(ethylene glycol) (MPEG) ($M_n$ = 750), tin(II) 2-ethylhexanoate ($Sn(Oct)_2$), and dexamethasone 21-phosphate disodium salt (Dex) were purchased from Sigma-Aldrich (United States of America [USA]). ε-caprolactone was obtained from TCI Chemicals (Japan) and distilled over calcium hydride under reduced pressure. L-lactide (Boehringer Ingelheim, France) was purified via two recrystallizations using ethyl acetate. Chloroform-D was purchased from Cambridge Isotope Laboratories, Inc. (USA). Toluene, dichloromethane, n-hexane, ethyl ether, and acetone were purchased from Samchun (Korea). Formalin (10%) and ethanol (100%) were obtained from Sigma-Aldrich. Mayer's hematoxylin solution was purchased from Corning (USA), and the anti-cluster of differentiation (CD) 68 antibody (ED1

antibody; AB303565) was obtained from Abcam (United Kingdom [UK]).

### 2.2. Synthesis and characterization of CL polymer inks

All glassware was heat-treated and vacuum-dried prior to use to eliminate residual moisture and contaminants. For the synthesis of the CL1 polymer ink, MPEG (0.075 g, 0.1 mmol) was placed in a pre-dried flask under a nitrogen atmosphere and dissolved in 90 mL of toluene. Azeotropic distillation was carried out at 150°C for 3 h to remove residual moisture. After distilling off 40 mL of toluene, ε-caprolactone (4.937 g, 43.254 mmol) and L-lactide (0.063 g, 0.437 mmol) were added to the flask. Subsequently, 0.2 mL of 0.1 M $Sn(Oct)_2$ solution was introduced as the catalyst, and ring-opening polymerization was conducted at 130°C for 24 h.

Following polymerization, the resulting copolymer was precipitated in a n-hexane/diethyl ether mixture (v/v = 4:1) to remove unreacted monomers and byproducts. The precipitate was then dissolved in dichloromethane, filtered, and concentrated using a rotary evaporator. The final CL1 polymer ink was obtained through vacuum drying to eliminate residual solvents.

Other CL polymer inks were synthesized using the same protocol with varying monomer feed ratios. The chemical composition and molecular weight of the synthesized polymer inks were characterized by proton nuclear magnetic resonance spectroscopy ($^1$H NMR). The molar ratio of L-lactide to ε-caprolactone was determined by integrating the characteristic peaks: methoxy protons of MPEG ($\delta$ = 3.38 ppm), methine protons of PLA ($\delta$ = 5.2 ppm), and methylene protons of PCL ($\delta$ = 2.3 ppm). The resulting compositions, designated as CL0 ($C_{100}L_0$), CL1 ($C_{99}L_1$), CL2 ($C_{91}L_9$), CL3 ($C_{85}L_{15}$), and CL4 ($C_{78}L_{22}$), were verified by $^1$H NMR analysis, which showed that the polymers were obtained with ratios closely matching the intended feed compositions.

Molecular weight and polydispersity index were measured using gel permeation chromatography (GPC) on a Futecs GPC 500 system (Korea) equipped with a Shodex 201H refractive index detector (Shoko Scientific, Japan). Separation was performed using Shodex K-802, K-803, and K-804 polystyrene gel columns with $CHCl_3$ as the eluent, at a flow rate of 1 mL/min and a column temperature of 40°C.

Thermal properties, including the $T_m$ and enthalpy of fusion ($\Delta H_m$), were analyzed via differential scanning calorimetry (DSC) using a DSC 25 system (TA Instruments, USA). Approximately, 4 mg of each sample was sealed in an aluminum pan. For thermal analysis, the samples were heated from −80 to 200°C at a rate of 10°C/min, cooled back to −80°C at the same rate, and then reheated to 200°C. This cycle was used to eliminate thermal history and ensure reproducibility of thermal transitions.

### 2.3. Thermal stability assessment of CL polymer inks

To assess the thermal stability and processing feasibility of the CL polymer inks for 3D printing applications, 0.3 g of each sample was placed in a 4 mL glass vial and subjected to controlled heating at 25, 40, 60, 80, 100, and 120°C for either 1 or 2 h. Following thermal exposure, the samples were cooled to room temperature before analysis. The molecular weight distribution of the heat-treated polymer inks was analyzed by GPC, as described previously, to identify any signs of thermal degradation or structural alteration in the polymers.

### 2.4. Rheological characterization of CL polymer inks

The rheological properties of the CL0 to CL4 polymer inks were evaluated using a rheometer (MCR 102, Anton Paar, Germany) equipped with a temperature-controlled Peltier lower plate and a stainless-steel parallel plate geometry (25.0 mm diameter). The gap between the plates was fixed at 0.2 mm for all measurements, which were conducted at 80 and 100°C.

For the time sweep test, measurements were performed over a time range of 0–600 s with an oscillation frequency of 1 Hz, a gamma amplitude of 0.1%, and an oscillatory strain of 1%. For the strain sweep test, the strain range was set to 0–1000% with a gamma amplitude of 0.1% and a frequency of 1 Hz. For the linear ramp test, viscosity was measured over a shear rate range of 0–100 $s^{-1}$. The storage modulus ($G'$), strain ($\gamma$, %), shear rate ($s^{-1}$), and viscosity (Pa s) were calculated using the instrument's built-in software.

### 2.5. *In vitro* biodegradation of CL polymer inks

The *in vitro* biodegradation behavior of the CL polymer inks was evaluated by placing 0.1 g of each sample into a glass vial containing 5 mL of distilled water (DW). The vials were sealed and incubated at 50°C with continuous shaking at 100 rpm for 4 weeks. After incubation, the samples were sequentially frozen at −10°C for 24 h and −80°C for an additional 48 h to prepare for freeze-drying. Lyophilization was subsequently carried out to ensure complete drying.

The freeze-dried polymer inks were dissolved in chloroform, filtered to remove any undissolved residues, concentrated using a rotary evaporator, and vacuum-dried for 4 days. The recovered polymers were then analyzed using GPC to assess changes in molecular weight and the extent of degradation. Additionally, $^1$H NMR spectroscopy was performed to investigate structural modifications in the CL copolymer backbone resulting from degradation.

### 2.6. Preparation of Dex-CL polymer inks

Dex-CL polymer inks were prepared by dissolving 1 g of each CL formulation (CL0, CL1, CL2, CL3, or CL4) in 30 mL of dichloromethane, while Dex was separately dissolved in 30 mL of acetone. These formulations correspond to the following monomer feed ratios: CL0 ($C_{100}L_0$), CL1 ($C_{99}L_1$), CL2 ($C_{91}L_9$), CL3 ($C_{85}L_{15}$), and CL4 ($C_{78}L_{22}$), as described in **Section 2.2**. The Dex solution was then combined with the corresponding CL solution, followed by thorough mixing to ensure uniform distribution of Dex within the CL matrix. The resulting mixture was subjected to rotary evaporation under reduced pressure at room temperature to remove the majority of the organic solvents, followed by additional vacuum drying at 40°C for 48 h to ensure complete elimination of any residual dichloromethane, acetone, or other volatile components. The absence of residual solvent was confirmed by $^1$H NMR spectroscopy, which showed no detectable solvent peaks in the final polymer ink samples. The dried, homogeneous Dex-loaded CL polymer inks were then utilized for subsequent FDM 3D printing. CL4 ($C_{78}L_{22}$) was excluded from further drug-loading and printing experiments due to its relatively low mechanical stability and rapid softening at the optimized printing temperatures, which could compromise structural fidelity.

### 2.7. 3D printing process and printability assessment

Polymer ink depots were fabricated using a solid freeform fabrication 3D plotter (Protek Korea, Korea) equipped with a heating chamber, a stainless-steel syringe, and a micronozzle (200 μm internal orifice, 0.4 mm outer diameter). Material deposition along the *x*-, *y*-, and *z*-axes was precisely controlled via an air pressure-driven dispensing mechanism. Depot geometries were designed using Depot Path Generation software (Korea Institute of Machinery and Materials, Korea) to ensure uniform and reproducible structural specifications.

Each polymer ink formulation was loaded into the upper chamber of the FDM system, and the chamber temperature was adjusted between 80 and 120°C according to the thermal characteristics of the respective formulation. Printing was performed in a layer-by-layer manner onto a substrate maintained at 23–25°C, yielding circular depots (5 mm diameter, 1 mm height) with an internal pore size of 300 μm. Printing speed (50–400 mm/min) and extrusion pressure (100–500 kPa) were optimized to ensure continuous filament deposition, accurate layer stacking, and high geometric fidelity. A micronozzle (200 μm internal orifice, 0.4 mm outer diameter) was used for all prints.

After the printing process, the printed depots were cooled and solidified at ambient temperature. Printability was assessed by measuring filament widths and internal pore dimensions at multiple random locations using ImageJ software (Wayne Rasband, USA). Deviations from the designed line width and pore area were calculated to quantify structural accuracy and reproducibility. These metrics were used to determine the suitability of each CL polymer ink formulation for FDM-based 3D printing of drug delivery depots.

### 2.8. 3D printing of Dex-CL depots and post-printing evaluation

For the fabrication of Dex-CL depots, 1 g of each prepared polymer ink was loaded into the heating chamber of the 3D printer. The printing temperature was set 10–30°C above the $T_m$ of the respective polymer ink to ensure smooth extrusion while maintaining structural integrity. Printing was conducted using a micronozzle (200 μm internal orifice, 0.4 mm outer diameter) at a feed rate of 400 mm/min and an extrusion pressure of 500 kPa. To ensure reproducibility, each formulation was printed in triplicate batches, with a minimum of 10 replicates per condition. Structural consistency was assessed by measuring dimensional accuracy and evaluating the uniformity of layer deposition. The printing time for a single Dex-CL depot was approximately 3 min. Additionally, the Dex and CL mixture was stored at 100°C for 2 h, and subsequent $^1$H NMR analysis revealed no significant structural changes.

Following fabrication, the printed depots were incubated at 25°C (ambient) and 37°C (physiological) for 6 h to assess thermal stability under relevant environmental conditions. Structural changes were monitored using optical microscopy and scanning electron microscopy (SEM; JSM-7900F, JEOL, Japan). SEM was used to evaluate surface morphology, pore architecture, and microstructural integrity, providing insights into physical features that could influence subsequent drug release behavior.

### 2.9. Encapsulation efficiency and *in vitro* Dex release from Dex-CL depots

The encapsulation efficiency and *in vitro* release profiles of Dex from Dex-CL depots were quantified using high-performance liquid chromatography (HPLC; 1200 Series, Agilent Technologies, USA). Chromatographic separation was performed on a Hypersil C18 column (4.6 mm; Agilent Technologies, Germany) with a mobile phase consisting of acetonitrile (ACN) and DW (60:40, v/v) at a flow rate of 1.0 mL/min. Dex was detected and quantified based on its retention time and a standard calibration curve prepared in phosphate-buffered saline (PBS, pH 7.4).

To determine the encapsulation efficiency of Dex in the Dex-CL depots, freeze-dried Dex-CL samples were dissolved in 0.5 mL of ACN and stirred continuously at room temperature for 10 min. Subsequently, 0.5 mL of

DW was added, and the mixture was vortexed thoroughly for an additional 10 min to ensure complete extraction of Dex from the polymer matrix. The resulting solution was filtered through a 0.22 μm syringe filter to remove undissolved polymer residues. The encapsulation efficiency was calculated using the following equation:

$$(\text{weight of Dex in Dex-CL/weight of Dex initially fed}) \times 100 \quad \text{(I)}$$

For the release study, circular Dex-CL depots (5 mm diameter, 1 mm height) were individually immersed in 3 mL of PBS (pH 7.4) in 4 mL vials and incubated at 37°C with continuous agitation (100 rpm) to mimic physiological conditions. At predetermined intervals over the 4-week study period, 1 mL of the release medium was withdrawn and immediately replaced with fresh PBS within 10 s to maintain sink conditions. All experiments were conducted in triplicate ($n$ = 3). Dex concentrations in the collected samples were quantified using HPLC (1200 Series, Agilent Technologies, USA) under the same chromatographic conditions described above. Cumulative release profiles were calculated based on the measured Dex concentrations and are presented as mean ± standard deviation.

### 2.10. *In vivo* implantation and evaluation of CL and Dex-CL depots

All animal experiments were approved by the Institutional Animal Care and Use Committee of Ajou University School of Medicine (Approval No. 2024-0030) and conducted in accordance with institutional ethical guidelines. Six-week-old male Sprague–Dawley (SD) rats (280–300 g; total $n$ = 36) were used to evaluate the *in vivo* biocompatibility and drug release behavior of CL and Dex-CL depots. No experiments involving human subjects were conducted in this study.

Anesthesia was induced via intraperitoneal injection of tiletamine–zolazepam (Zoletil™ 50; Virbac, France) combined with xylazine (Rompun; Bayer Korea, Korea). After shaving and disinfecting the surgical site with povidone–iodine, the depots (5 mm diameter, 1 mm in height) were implanted into the subcutaneous tissue via a small incision. All depots were sterilized using ethylene oxide gas prior to implantation. Incisions were closed with absorbable sutures, and animals were housed under standard laboratory conditions with free access to food and water. At designated time points, rats were euthanized via carbon dioxide inhalation following institutional protocols. Implanted depots were retrieved for evaluation of drug release kinetics, structural integrity, degradation, and histological response, enabling a comprehensive assessment of *in vivo* performance.

### 2.11. Morphological and drug release analyses of *in vivo* Dex-CL depots

At designated post-implantation time points (Weeks 1, 2, 3, and 4), rats were euthanized, and the subcutaneously implanted Dex-CL depots were carefully excised from the dorsal region for subsequent morphological, structural, and drug release evaluations. All experiments were conducted in triplicate ($n$ = 3) at each predetermined interval during the 4-week study period.

For morphological assessment, the retrieved depots were initially examined using a Camscope system (Sometech, Korea) and an optical microscope (Labophot-2, Nikon, Japan) at magnifications of 100× and 300×. Fine structural features were further analyzed using field-emission SEM, as previously described in **Section 2.8**. To preserve native morphology, the samples were flash-frozen in liquid nitrogen and lyophilized at −75°C for 5 days. The depots were then cryosectioned under liquid nitrogen to minimize structural disruption. Prior to SEM imaging, samples were gold-coated using a PS-1200 plasma sputter coater (Para One, Korea) under an argon atmosphere.

To quantify the residual Dex content in the depots, surface-adhered tissue was gently removed. Each depot was placed in a test tube containing 8 mL of ACN, homogenized at 16,000 rpm for 10 min at 25°C, and subsequently sonicated at the same temperature for 30 min. The homogenate was then centrifuged at 2000 rpm for 10 min at 4°C, and the supernatant was filtered through a 0.45 μm polytetrafluoroethylene membrane. ACN was removed by rotary evaporation under reduced pressure, and the resulting residue was reconstituted and analyzed by HPLC, as previously described in **Section 2.9**. Dex concentrations were determined using calibration curves prepared from known standards. All *in vivo* drug release experiments were independently conducted in three rats per condition, and results are expressed as mean ± standard deviation. These analyses provided comprehensive insights into depot morphology, *in vivo* structural stability, and Dex release kinetics over the 4-week period.

### 2.12. Histological and immunohistochemical analysis of host tissue response

At 2 and 4 weeks post-implantation, Dex-CL depots were explanted along with the surrounding tissues, which were immediately fixed in 10% neutral-buffered formalin to preserve morphology. The fixed tissues were processed into paraffin blocks, and 5 μm-thick sections were prepared using a microtome. The slides were incubated at 60°C for 2 h to ensure complete paraffin removal.

For hematoxylin and eosin (H&E) staining, deparaffinization was performed by immersing the slides in xylene for 10 min. It is important to note that during xylene treatment, the CL polymer inks were completely dissolved and removed, leaving only the host tissue for histological evaluation. This was followed by rehydration through a graded ethanol series (100%, 95%, 90%, 80%, and 70%; 10 min each). Sections were then stained with Harris hematoxylin (Sigma, USA) for 5 min, rinsed with DW for 2 min, and counterstained with 20% eosin solution (Sigma) for 5 min. After a final rinse in DW (1 min), the sections were dehydrated sequentially in ethanol (70–100%; 30 s each) and mounted using a permanent mounting medium (Muto Pure Chemicals, Japan).

For immunohistochemical staining of ED1 (CD68), paraffin sections were similarly deparaffinized and rehydrated. Antigen retrieval was conducted using citrate buffer (Sigma) at 120–130°C for 10 min, followed by cooling and two washes in PBS (5 min each). The slides were then incubated in PBST (0.05% Tween 20 in PBS) for 10 min. To block non-specific binding, the sections were treated with 5% horse serum (HS; Gibco, New Zealand) and 5% bovine serum albumin (BSA; Bovogen, Australia) in PBS for 90 min at 37 °C.

The primary antibody, mouse anti-rat CD68 (ED1; Abcam, UK), was diluted 1:1000 in antibody diluent (DAKO, Denmark) and applied overnight at 4°C. After washing twice with PBS and once with PBST, the sections were incubated with goat anti-mouse immunoglobulin G conjugated with Alexa Fluor 594 (Invitrogen, USA), diluted 1:200 in 1% BSA, for 3 h at room temperature. Nuclear counterstaining was performed using ProLong™ Gold Antifade Reagent with 4',6-diamidino-2-phenylindole (DAPI; Life Technologies, USA). The slides were mounted and visualized using an Axio Imager A1 fluorescence microscope (Carl Zeiss Microimaging GmbH, Germany), and images were acquired using Axiovision software (Rel. 4.8). Quantitative analysis of ED1-positive cells was performed using ImageJ, with data averaged from three specimens per group ($n = 3$). These evaluations provided detailed insights into tissue morphology and immune cell infiltration surrounding the implanted depots (Figure 1).

### 2.13. Statistical analyses

All data are presented as mean ± standard deviation from three independent experiments. Statistical comparisons were performed using one-way analysis of variance followed by Bonferroni's post hoc test for multiple comparisons. Analyses were conducted using SPSS version 12.0 (SPSS Inc., USA). A $p$-value of less than 0.05 was considered statistically significant.

## 3. Results

### 3.1. Synthesis of CL polymer inks

ε-caprolactone polymer inks were successfully synthesized by incorporating 1–20 mol% of PLA into the PCL backbone of the copolymers, yielding copolymers with an average molecular weight of approximately 50,000 g/mol. As summarized in Table 1, the resulting polymer inks were colorless and exhibited precipitation yields exceeding 90%. The $^1$H NMR spectra displayed characteristic peaks corresponding to PCL, PLA, and MPEG, confirming the successful random incorporation of all monomeric units (Figure 2A). Moreover, the molecular weights and compositional ratios of PCL and PLA, calculated from signal integration in the $^1$H NMR spectra, closely matched the theoretical feed ratios. These findings demonstrate the successful synthesis of CL-based copolymers with precisely controlled PCL and PLA contents, supporting their potential as tunable polymer inks for biomedical applications.

### 3.2. Thermal characterization of CL polymer inks for fused deposition modeling 3D printing

To assess their thermal suitability for FDM 3D printing, DSC was performed on CL copolymers containing 1–20 mol% PLA. The DSC analysis revealed no melting peaks near 175°C, the typical $T_m$ of crystalline PLA, suggesting a high degree of phase compatibility between the PCL and PLA segments despite their random incorporation.

As shown in Table 1 and Figure 2B, both the $T_m$ and the enthalpy of fusion ($\Delta H_m$) decreased progressively with increasing PLA content. Specifically, $T_m$ decreased from approximately 56 to 40°C, while $\Delta H_m$ declined from 60 to 17 J/g. These results indicate that increasing PLA content disrupts the crystalline order of the PCL matrix, thereby lowering its thermal transition parameters.

Among the tested CL copolymers, CL4 exhibited the lowest $T_m$ (~40°C), approaching physiological temperature (~38°C), suggesting potential softening or partial dissolution under biological conditions.

Overall, these results demonstrate that the thermal behavior of CL-based copolymers can be precisely tuned by adjusting the PLA content. This thermal tunability offers a strategic advantage for optimizing printability and functional performance in FDM-based drug delivery systems.

### 3.3. Thermal stability of CL polymer inks under fused deposition modeling 3D printing conditions

The thermal stability of CL polymer inks was evaluated to determine their suitability for FDM 3D printing. For effective printing, polymer inks must melt efficiently within the heating chamber, flow smoothly through the nozzle

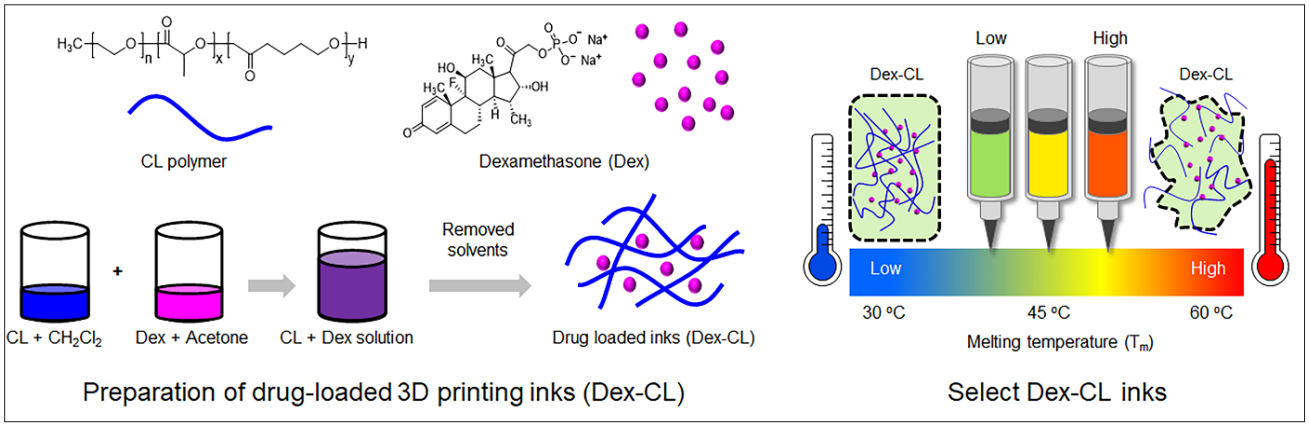


**Figure 1.** Schematic representation of the fabrication process for 3D-printed CL depots loaded with Dex. Abbreviations: CL, poly(ε-caprolactone-ran-lactide); Dex-CL, dexamethasone-loaded CL.

**Table 1. Preparation and characterization of poly(ε-caprolactone-ran-lactide) (CL) polymer inks**

| No. | Theory molar ratio (%) [C:L][a] | Obtained molar ratio (%) [C:L][b] | MW[b] | $T_m$ (°C)[c] | $\Delta H$ (J/g)[c] | Yield (%) | $M_w/M_n$[d] | Printability |
|---|---|---|---|---|---|---|---|---|
| CL0 | $C_{100}L_0$ | $C_{100}L0$ | 50,000 | 56.0 | 60.2 | 95 | 1.1 | O |
| CL1 | $C_{99}L_1$ | $C_{99}L_1$ | 56,000 | 55.1 | 58.7 | 90 | 1.3 | O |
| CL2 | $C_{90}L_{10}$ | $C_{91}L_9$ | 51,000 | 47.3 | 48.2 | 91 | 1.2 | O |
| CL3 | $C_{84}L_{16}$ | $C_{85}L_{15}$ | 50,000 | 41.9 | 32.5 | 90 | 1.2 | O~Δ |
| CL4 | $C_{80}L_{20}$ | $C_{78}L_{22}$ | 52,000 | 39.7 | 17.3 | 93 | 1.3 | Δ~X |

Abbreviations: $M_n$, number average molecular weight; MW, molecular weight; $M_w$, weight average molecular weight; O, (**High fidelity**: accurate line width and well-defined pores); O~Δ, (**Moderate fidelity**: acceptable line width and pore structure, with minor deviations from design); $T_m$, melting point; Δ*H*, enthalpy of fusion; Δ~X, (**Low fidelity**: a irregular or collapsed line width and pores, resulting in poor structural definition).

[a]C: ε-caprolactone, L: L-Lactide.

[b]Determined by proton nuclear magnetic resonance spectroscopy.

[c]Determined by differential scanning calorimetry.

[d]Measured by gel permeation chromatography, using polystyrene standards.

under pressure, and solidify into a stable 3D structure at room temperature (23–25°C). To assess thermal resistance, CL polymer inks were incubated in the printer chamber at various temperatures for 2 h. GPC analysis (Figure 2C) showed negligible changes in molecular weight, even after exposure to temperatures up to 120°C. These results confirm the excellent thermal stability of CL polymer inks, indicating resistance to heat-induced degradation and preservation of molecular characteristics throughout the printing process.

This thermal stability is essential for maintaining the structural integrity and reproducibility of printed constructs in biomedical applications. Collectively, these findings demonstrate that CL polymer inks are well-suited for use in temperature-sensitive FDM printing processes, particularly in the fabrication of drug delivery systems.

### 3.4. Rheological evaluation of CL polymer inks at printing temperatures

To predict the flowability and printability of CL0–CL4 polymer inks under FDM 3D printing conditions, rheological behaviors at 80, 100, and 120°C were analyzed using time sweep, strain sweep, and linear ramp measurements (Figure 3).

In the time sweep measurements, *G*' values were consistently lower at elevated temperatures (100 and 120°C) compared to 80°C, indicating that higher thermal input weakens the intermolecular interactions between polymer chains within the CL polymer inks. Nevertheless, all polymer inks maintained relatively stable *G*' values throughout the measurement period, suggesting that their viscoelastic integrity was preserved over time.

The strain sweep results revealed that across all tested temperatures, CL0 and CL1 exhibited a rapid decrease

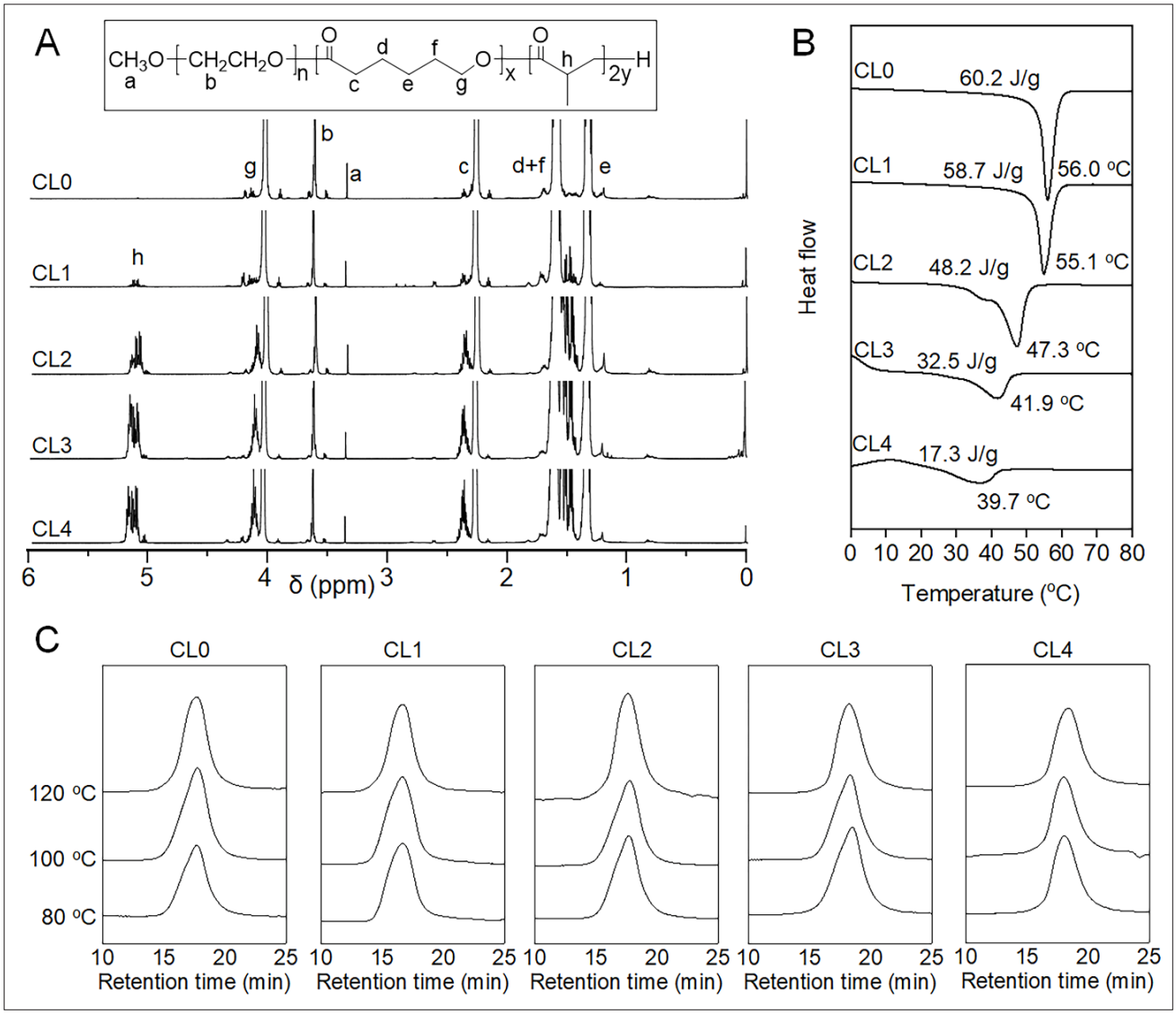


**Figure 2.** Physicochemical characterization of CL0, CL1, CL2, CL3, and CL4 polymer inks. (A) Representative proton nuclear magnetic resonance spectroscopy spectra confirming the chemical composition and monomer ratio of each copolymer formulation. (B) Differential scanning calorimetry thermograms illustrating the thermal transitions and crystallinity profiles of the CL polymer inks. (C) Gel permeation chromatography profiles obtained after 2 h of heating at 80–120°C, demonstrating the thermal stability of each formulation based on changes in molecular weight distribution. Note: Molar ratio of L-lactide to ε-caprolactone for CL0 = $C_{100}L_0$, CL1 = $C_{99}L_1$, CL2 = $C_{91}L_9$, CL3 = $C_{85}L_{15}$, and CL4 = $C_{78}L_{22}$. Abbreviation: CL, poly(ε-caprolactone-ran-lactide).

in *G*' at low strain levels, whereas CL2 showed a smaller initial drop. In contrast, CL3 and CL4 maintained nearly constant *G*' values across the entire strain range. This behavior can be attributed to the higher lactide content in CL3 and CL4, which reduces crystallinity and increases chain flexibility, thereby limiting the reduction in *G*' under increasing strain.

In the linear ramp tests, CL0 and CL1 showed a pronounced decrease in viscosity (Pa s) with increasing shear rate, consistent with their higher crystallinity and stronger chain entanglement at low shear rates. By contrast, CL2, CL3, and CL4—having higher lactide content, lower crystallinity, and weaker intermolecular interactions—exhibited only a modest additional decrease in viscosity. In all cases, viscosities were lower at elevated temperatures (100 and 120°C) than at 80°C, likely due to increased molecular mobility of polymer chains.

Overall, these findings indicate that both copolymer composition (CL:lactide ratio) and printing temperature strongly influence the flow behavior of the polymer inks

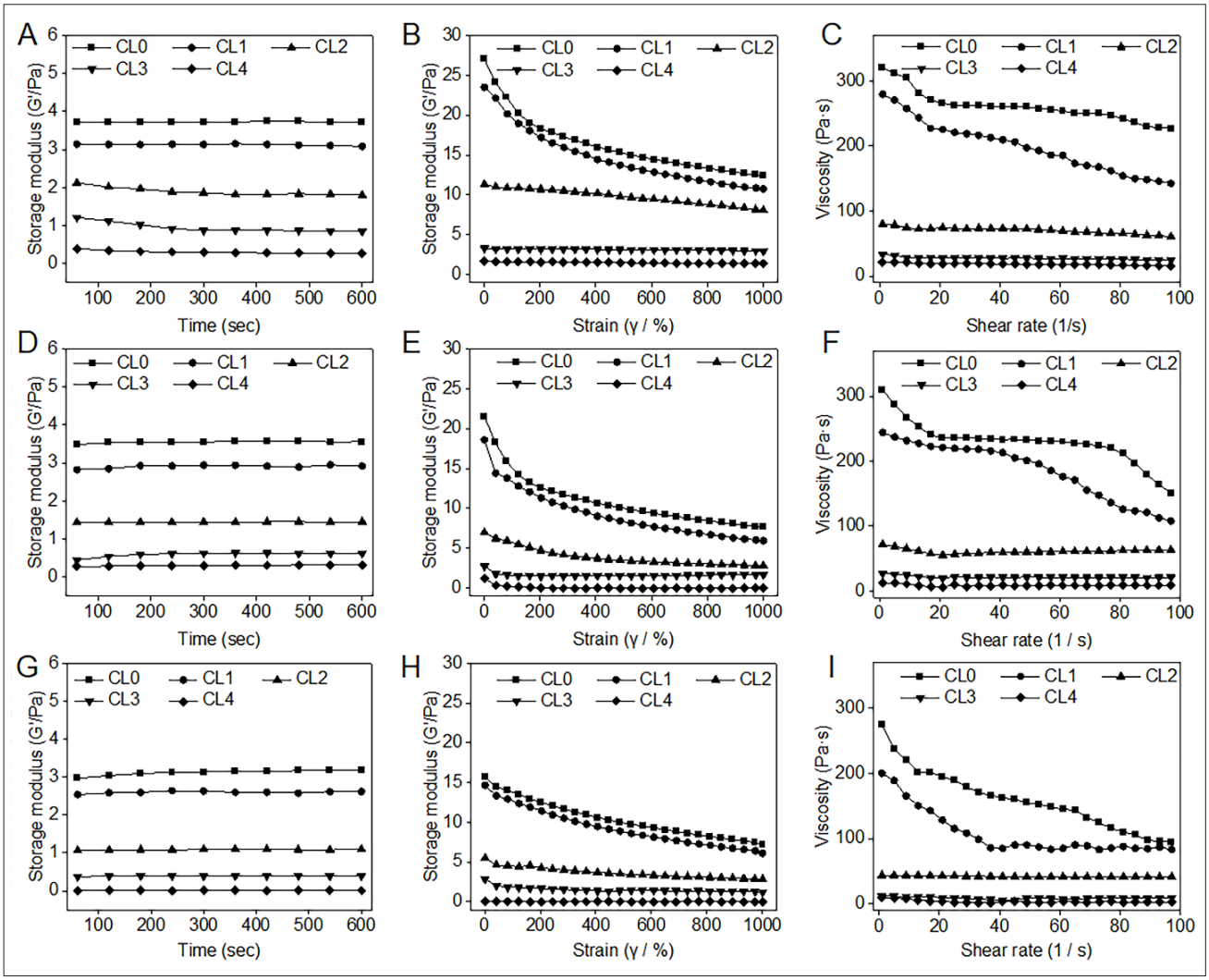


**Figure 3.** Rheological characterization of CL bioinks at (A–C) 80°C, (D–F) 100°C, and (G–I) 120°C. (A, D, G) Time sweep test; (B, E, H) strain sweep test; (C, F, I) linear ramp measurements. Note: Molar ratio of L-lactide to ε-caprolactone for CL0 = $C_{100}L_0$, CL1 = $C_{99}L_1$, CL2 = $C_{91}L_9$, CL3 = $C_{85}L_{15}$, and CL4 = $C_{78}L_{22}$. Abbreviation: CL, poly(ε-caprolactone-ran-lactide).

through the printer nozzle and the structural fidelity of the resulting printed constructs.

### 3.5. Printability and structural fidelity of CL polymer inks for fused deposition modeling 3D printing

The printability and structural fidelity of CL polymer inks were systematically evaluated to determine their suitability for FDM 3D printing (Figures 4 and S1, Supporting Information). Successful FDM printing requires that the polymer ink melts efficiently within the heating chamber, flows consistently under applied pressure, and rapidly solidifies at ambient temperature (23–25°C) to preserve the intended geometry. Variations in extrusion pressure or printing speed can affect line width and resolution. Therefore, optimizing these parameters is essential for high-fidelity fabrication.

First, the influence of chamber temperature was assessed across the 80–120°C range, previously verified to preserve the thermal stability of CL polymer inks. At temperatures below 80°C, extrusion was inconsistent and prone to nozzle clogging. At temperatures above 120°C, excessive fluidity led to over-extrusion, pore collapse, and yellow discoloration, likely due to thermal oxidation or degradation. It should be noted that the observed yellow discoloration at 120°C does not contradict the GPC results, indicating unchanged molecular weight distribution. GPC primarily detects polymer chain scission or crosslinking events, whereas discoloration can arise from minor thermo-

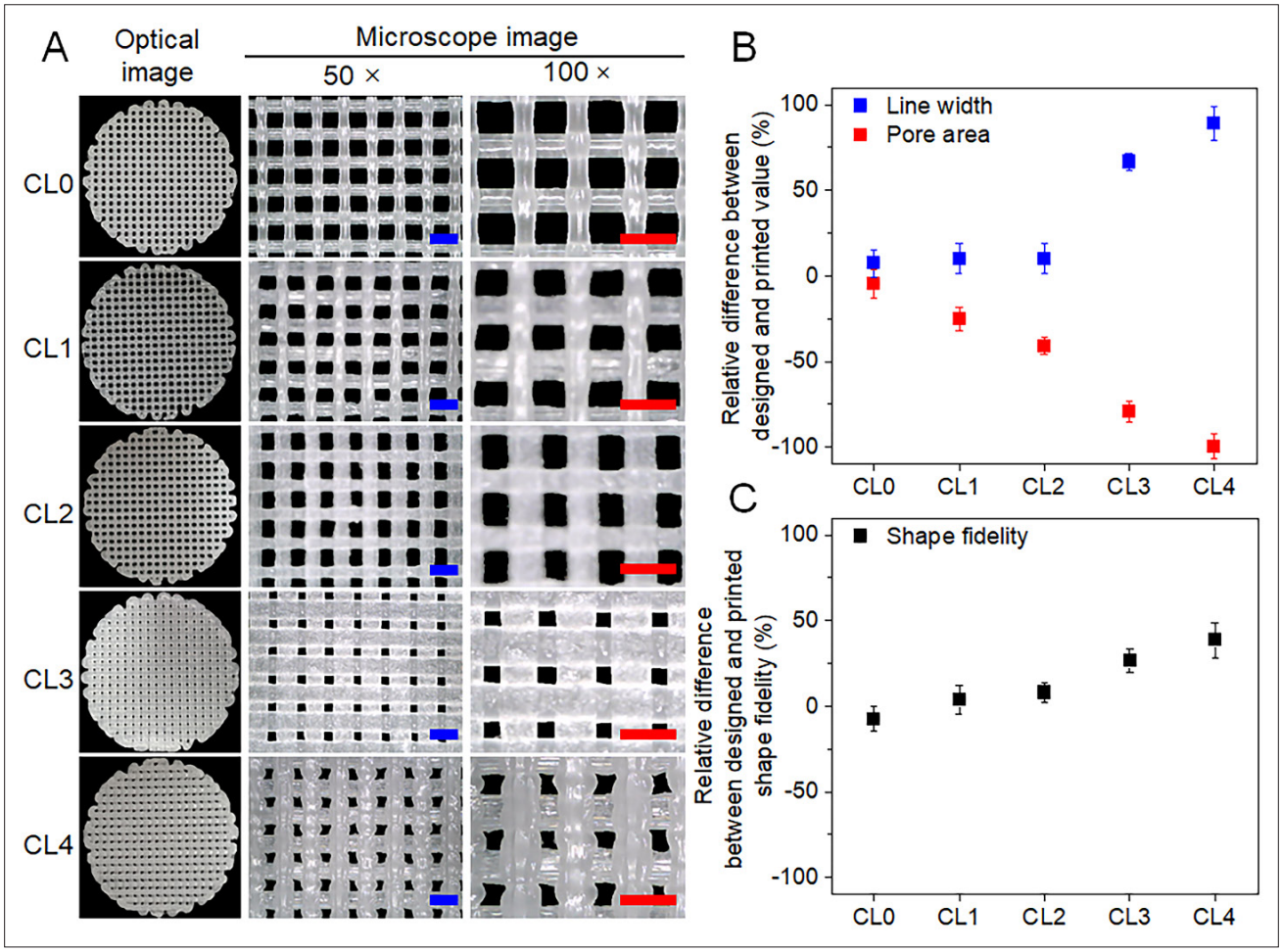


**Figure 4.** Printability and structural fidelity of CL polymer inks under fused deposition modeling 3D printing conditions. (A) Optical and microscopic images of 3D-printed CL polymer ink depots (CL0–CL3) showing strand morphology and pore architecture (scale bar = 1 mm; magnifications = 50× and 100×). (B) Quantitative comparison between designed and actual printed features, including relative deviations in line width and pore area, across different CL polymer inks. (C) Relative shape fidelity of printed depots, calculated by integrating the deviations in both line width and pore area. Note: Molar ratio of L-lactide to ε-caprolactone for CL0 = $C_{100}L_0$, CL1 = $C_{99}L_1$, CL2 = $C_{91}L_9$, CL3 = $C_{85}L_{15}$, and CL4 = $C_{78}L_{22}$. Abbreviation: CL, poly(ε-caprolactone-ran-lactide).

oxidative surface reactions, catalyst residue interactions, or trace impurity degradation—none of which necessarily alter the bulk chain length. These subtle chemical changes, while not impacting molecular weight, can still affect visual appearance and potentially surface-related performance.

During fabrication at the optimized chamber temperature of 100°C, individual DDS units required approximately 3–5 min of continuous heating from polymer ink loading to completion of printing. For multi-unit production runs, the copolymer–drug mixture remained in the heated chamber for up to 25 min, which was the longest duration tested under practical conditions. Notably, GPC analysis after simulated heating for 2 h at 100°C confirmed no detectable molecular weight degradation, indicating that all actual processing times in this study fell well within the thermally safe window for CL polymer inks.

Next, the effects of printing speed (50–400 mm/min) and extrusion pressure (100–500 kPa) were evaluated at a fixed chamber temperature of 100°C. Over-extrusion occurred at high pressure (500 kPa) and low speed (50 mm/min), while under-extrusion was observed at low pressure (100 kPa) and high speed (400 mm/min), highlighting the interdependent roles of pressure, polymer ink viscosity, and solidification rate during extrusion.

Optimal printing conditions were determined to be a chamber temperature of 100°C, an ambient platform temperature, a printing speed of 200 mm/min, and an extrusion pressure of 400 kPa. Under these conditions, drug delivery depots with a designed pore size of 300 μm

and a line width of 350 μm were fabricated using different CL formulations (CL0–CL4). Structural fidelity was evaluated based on the measured line width and pore area of the printed depots (Figure 4). Representative optical microscopic images (Figure 4A) showed that CL0, CL1, and CL2 produced stable geometries closely matching the designed specifications (Figure 4B). In contrast, CL3 and CL4 displayed excessive material extrusion due to lower viscosities, leading to an 80–90% increase in line width and a >60 % reduction in pore area, resulting in near-complete pore collapse.

These deviations in printed geometry are not merely superficial but critically impact the microarchitecture of the drug delivery depots—including pore size uniformity, interconnectivity, and surface-to-volume ratio. Such structural parameters govern drug diffusion and degradation-mediated release rates. Excessive widening of printed lines or pore collapse (as observed in CL3 and CL4) reduces effective surface area and alters internal diffusion pathways, leading to slower or less predictable release kinetics. Conversely, high-resolution, dimensionally accurate prints (CL0–CL2) preserve the designed porosity and geometry, ensuring consistent drug loading distribution and predictable release profiles throughout the intended therapeutic period. Under these optimized printing conditions, the dimensional accuracy of CL0–CL2 remained within ±10% of the design, indicating minimal geometry-induced variation in internal surface area. This suggests that, for high-fidelity prints, drug release kinetics are primarily dictated by the CL polymer ink composition and degradation behavior, with geometry-related effects being negligible.

It is well recognized that the geometry of 3D-printed depots can modulate drug release by altering the surface-to-volume ratio and diffusion pathways. In our study, the printing fidelity of CL0–CL2 formulations ensured near-identical pore architecture and line width, minimizing geometry-driven variability. Consequently, the *in vitro* release profiles primarily reflect the intrinsic degradation and diffusion characteristics of each CL polymer ink, rather than differences in printed geometry. This supports the interpretation that, under the optimized FDM parameters, the controlled nature of the DDS arises from material properties, with geometry effects held constant.

Shape fidelity analysis further confirmed that CL0–CL2 maintained 90–100% fidelity, with dimensional accuracy within ±10% of design values (Figure 4C), whereas CL3 and CL4 deviated substantially due to excessive flow and low mechanical integrity of the extruded lines. Collectively, these results demonstrate that the PCL-to-PLA ratio critically influences print performance, and that precise control of copolymer composition, alongside optimized printing parameters, is essential for achieving reproducible, high-resolution 3D-printed drug delivery depots. Among all formulations, CL4 exhibited the poorest printability, characterized by filament collapse, fused layers, and structural distortion—effects attributed to its low $T_m$ and excessively low viscosity. These deficiencies, along with its thermal instability during FDM-based printing and observable clumping and deformation at physiological temperatures, led to its exclusion from further experiments, as it was deemed unsuitable for use as a stable implantable drug carrier.

### 3.6. *In vitro* biodegradation behavior of CL polymer inks

In our previous study, CL polymers showed almost no degradation at 37°C even after 14 weeks.[20] Building on this observation, the present study investigated the *in vitro* biodegradation profiles of CL polymer inks with varying PCL-to-PLA molar ratios at 37°C (physiological conditions), as well as at 50°C, where accelerated degradation enabled clearer assessment of compositional effects.

First, GPC analysis demonstrated that the molecular weights of the CL polymer inks remained largely unchanged across all formulations, suggesting that bulk degradation was minimal during the incubation period.

In contrast, $^1$H NMR provided greater sensitivity to subtle chemical alterations. CL0 showed no detectable structural changes at either temperature, confirming its high chemical stability (Figures 5 and S2, Supporting Information). CL1 and CL2 exhibited minor but noticeable spectral changes at 4.45 and 1.55 ppm, with CL2 showing a more pronounced additional peak at 50°C. These low-intensity signals, although minor compared to the major intact polymer peaks, suggest partial hydrolytic cleavage of lactide-derived segments. Importantly, CL3 demonstrated an even stronger degradation pattern than CL2, particularly at 50°C, which can be attributed to its higher lactide content, reduced crystallinity, and increased hydrophilicity—factors that collectively enhance water uptake and accelerate hydrolysis.

Collectively, these findings demonstrate that the *in vitro* degradation behavior and structural integrity of CL polymer inks are governed by copolymer composition. This underscores the compositional tuning as a key design strategy, enabling the development of CL-based polymer inks with tailored biodegradation profiles.

### 3.7. Preparation and characterization of 3D-printed Dex-CL depots

To fabricate printable drug delivery depots and evaluate their drug-loading performance, Dex was incorporated

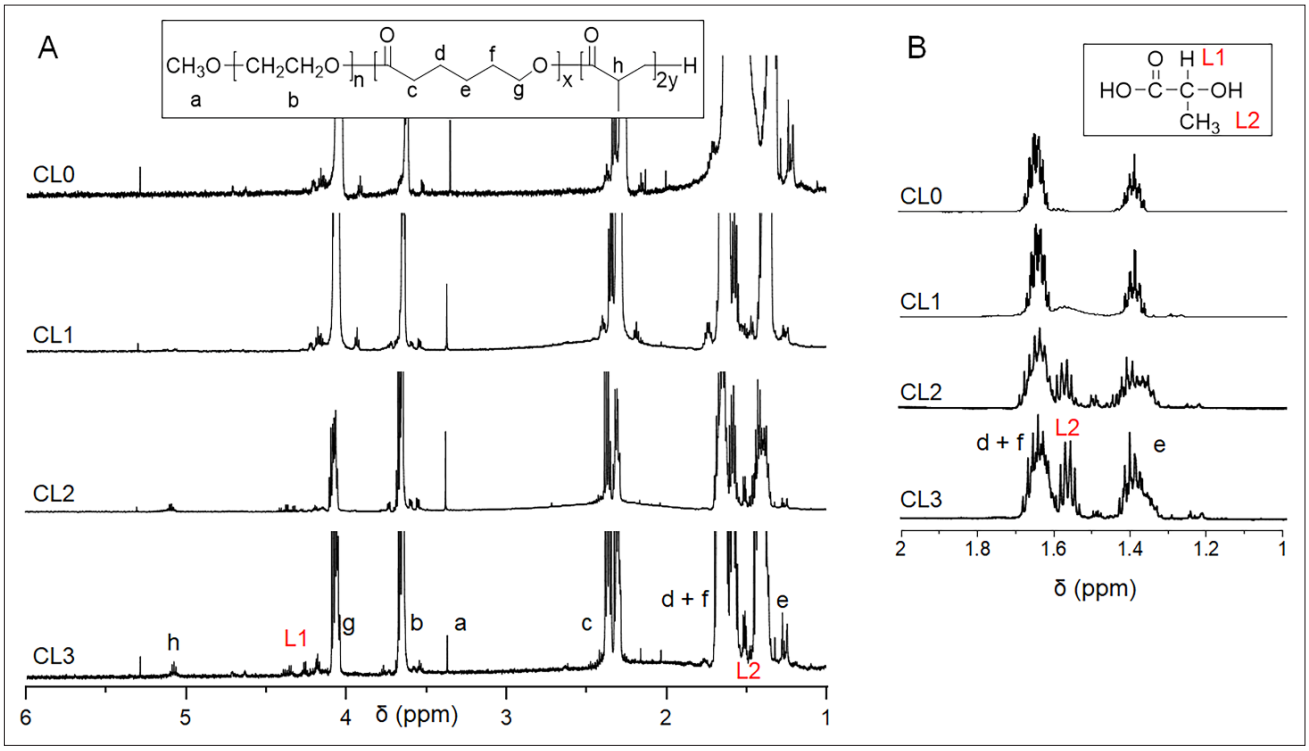


**Figure 5.** Hydrolytic degradation analysis of CL0, CL1, CL2, and CL3 polymer inks via proton nuclear magnetic resonance spectroscopy ($^1$H NMR) after incubation in distilled water at 50°C. (a) Full $^1$H NMR spectra of the incubated samples, showing the overall chemical structure of each formulation. (b) Magnified view of the L2 region (1.0–2.0 ppm), highlighting the methyl proton signals of lactide units to assess hydrolytic cleavage and degradation behavior over time. Note: Molar ratio of L-lactide to ε-caprolactone for CL0 = $C_{100}L_0$, CL1 = $C_{99}L_1$, CL2 = $C_{91}L_9$, and CL3 = $C_{85}L_{15}$. Abbreviation: CL, poly(ε-caprolactone-ran-lactide).

into CL0, CL1, CL2, and CL3 polymer ink powders at concentrations ranging from 1 to 5 wt% to produce homogeneous mixtures.

Differential scanning calorimetry analysis revealed that, similar to CL polymer inks, no melting peak appeared near 175°C, the typical $T_m$ of crystalline PLA. This indicates that the incorporation of Dex did not significantly alter the crystallization behavior within the CL copolymer matrix.

As shown in Table 2 and Figure S3, Supporting Information, all Dex-CL formulations exhibited slight decreases in both $T_m$ and $\Delta H_m$ upon incorporation of Dex. While Dex disrupted the crystallization of the CL polymer inks to some extent, thereby lowering thermal transition parameters, the magnitude of this effect was minimal. Collectively, these results suggest that the addition of Dex exerts only a negligible influence on the thermal behavior of CL polymer inks. Consequently, Dex can be effectively loaded without compromising the printability or functional performance of the depot formulations.

Each Dex-loaded CL formulation was subsequently processed in the heating chamber of the FDM printer and fabricated under the previously optimized thermal conditions to generate 3D-printed drug depots. As shown in Figure 6, all printed depots retained well-defined circular geometries and regular pore structures across all Dex concentrations. The depots were fabricated in a layer-by-layer orthogonal pattern according to a computer-generated design (5 mm diameter, 1 mm height), featuring strand widths of 200 μm and inter-strand pore sizes of 300 μm (top view). At ambient temperature (25°C), Dex-CL0, CL1, and CL2 depots successfully preserved their intended architectures. In contrast, Dex-CL3 depots showed minor filament deformation, such as partial fusion and strand flattening, likely due to their lower mechanical stability.

Among the tested formulations, Dex-CL2 demonstrated the highest consistency in maintaining pore structure and geometric fidelity across all Dex concentrations. Encapsulation efficiency was uniformly high for all groups, averaging approximately 90% (Figure 6E), confirming efficient drug incorporation and retention during the printing process.

To assess the stability of the printed depots under physiological conditions, samples were incubated at 37°C

**Table 2. Preparation and characterization of Dex-CL depots for printability**

| No. | Dex (wt%) | $T_m$ (°C)[a] | $\Delta H$ (J/g)[a] | Printability | Encapsulation[b] |
|---|---|---|---|---|---|
| CL0 | 3 | 53.4 | 57.3 | O | 95 |
| CL1 | 3 | 53.1 | 52.8 | O | 89 |
| CL2 | 1 | 46.1 | 46.4 | O | 91 |
| | 3 | 45.9 | 43.9 | | 93 |
| | 5 | 44.7 | 40.9 | | 88 |
| CL3 | 3 | 40.9 | 31.2 | O~Δ | 84 |
| CL4 | 3 | 37.9 | 15.8 | Δ~X | - |

Abbreviations: CL, poly(ε-caprolactone-ran-lactide); Dex, dexamethasone; Dex-CL, dexamethasone-loaded CL; O, (**high fidelity**: accurate line width and well-defined pores); O~Δ, (**moderate fidelity**: acceptable line width and pore structure, with minor deviations from design); Δ~X, (**low fidelity**: a irregular or collapsed line width and pores, resulting in poor structural definition).

[a]Determined by differential scanning calorimetry measurement.

[b]Determined by high-performance liquid chromatography.

for 6 h, followed by optical and SEM imaging (Figure 6B and D). Dex-CL0, CL1, and CL2 depots generally retained their original shapes and pore architectures, indicating excellent thermal and structural stability. In particular, Dex(3)-CL0, Dex(3)-CL1, Dex(1)-CL2, Dex(3)-CL2, and Dex(5)-CL2 displayed outstanding shape fidelity and uniform surface morphology, supporting their potential use as implantable sustained-release drug depots.

In contrast, Dex-CL3 depots exhibited complete filament fusion and significant pore collapse after incubation at 37°C. This behavior confirms that the low $T_m$ of CL3 (~40°C) compromises structural integrity under physiological conditions. However, this thermal sensitivity may be advantageous for rapid-release applications, where matrix dissolution is triggered at body temperature.

Collectively, these findings suggest that Dex-CL0, CL1, and CL2 depots offer sufficient mechanical robustness and thermal stability for sustained drug delivery. In contrast, CL3 may be better suited for scenarios requiring thermally responsive, rapid-release drug delivery systems.

### 3.8. *In vitro* Dex release from 3D-printed Dex-CL depots

The release behavior of Dex, incorporated as dexamethasone 21-phosphate disodium salt, was evaluated under

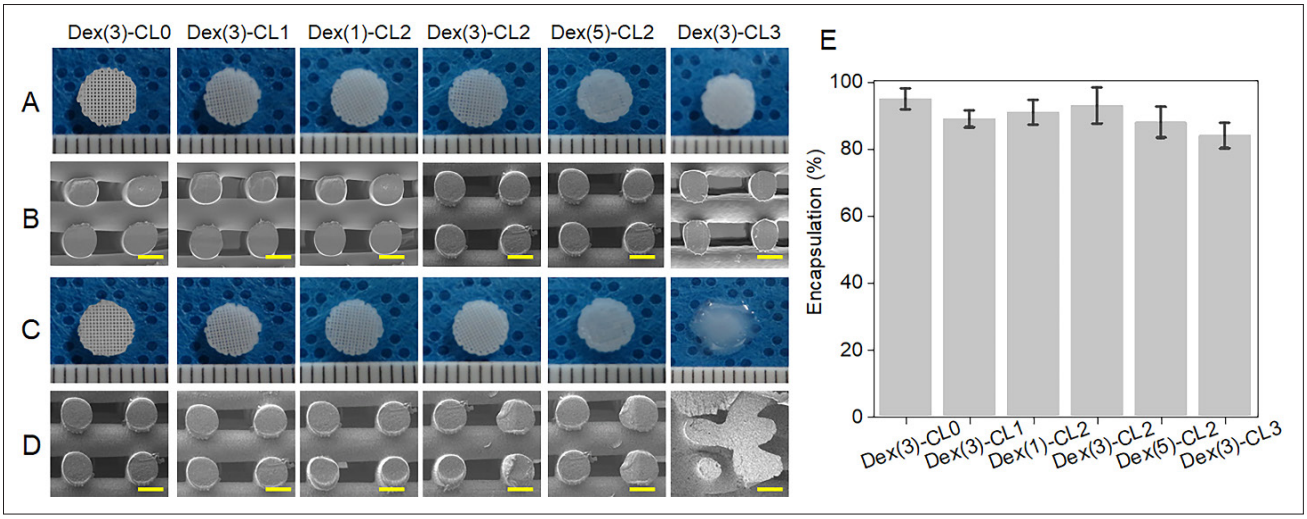


**Figure 6.** Characterization of 3D-printed Dex-CL depots. Optical photographs of Dex-CL depots incubated at (A) 25°C and (C) 37°C after 6 h of incubation. Scanning electron microscopy images of cross-sections of Dex-CL depots after 6 h of (B) 25°C and (D) 37°C incubation (scale bar = 100 μm; magnification = 100×), with numbers indicating the Dex concentration. (E) Encapsulation efficiency of Dex within the Dex-CL depots. Abbreviations: CL, poly(ε-caprolactone-ran-lactide); Dex-CL, dexamethasone-loaded CL.

physiological conditions. Given its hydrophilic nature, Dex release from the 3D-printed Dex-CL depots into PBS at 37°C was expected to occur through a combination of dissolution and diffusion mechanisms.

As shown in Figure 7, all Dex-CL depots exhibited sustained release profiles over a 30-day period, with minimal initial burst release. The early-phase release rate was influenced by the thermal properties of the CL polymer inks, particularly their $T_m$ relative to the incubation temperature. Depots fabricated with lower-$T_m$ polymer inks, such as CL3, showed a modestly accelerated initial release. However, following the early phase, all formulations converged toward similar sustained release profiles, demonstrating comparable long-term release behavior across all depot types.

Furthermore, the cumulative amount of Dex released increased proportionally with the initial loading concentration (1%, 3%, and 5%), indicating a clear dose-dependent release trend. These results underscore the importance of both the thermal characteristics of the polymer ink and the Dex loading level in modulating drug release kinetics. In summary, the 3D-printed Dex-CL depots enabled controlled and tunable drug release over extended durations, highlighting their potential for use in long-term therapeutic applications.

### 3.9. *In vivo* application of 3D-printed Dex-CL depot and Dex release profile

To evaluate the *in vivo* release kinetics and biocompatibility of 3D-printed Dex-CL depots, the constructs were subcutaneously implanted in SD rats and monitored over a 4-week period. The implantation procedure was well tolerated, with no observable adverse effects or signs of inflammation, indicating excellent biocompatibility of the CL polymer inks (Figure 8A).

Depot integrity was examined at 2 and 4 weeks post-implantation using optical and SEM imaging (Figure 8B and C). Most depots, especially those fabricated from Dex-CL0, CL1, and CL2, maintained their structural integrity throughout the study. Within the Dex-CL2 group, varying Dex concentrations did not result in noticeable morphological differences. In contrast, Dex-CL3 depots exhibited significant softening, filament fusion, and structural collapse by Week 2, attributed to their low $T_m$ (~40°C), which closely approaches physiological temperature and compromises *in vivo* stability.

Cumulative Dex release was measured at Weeks 1, 2, 3, and 4 (Figure 9). All depots with equivalent Dex loading showed an initial burst release during the first week, followed by sustained release over the remaining period. After 1 week, cumulative release reached approximately 18%, 22%, and 38% for Dex-CL1, CL2, and CL3 depots,

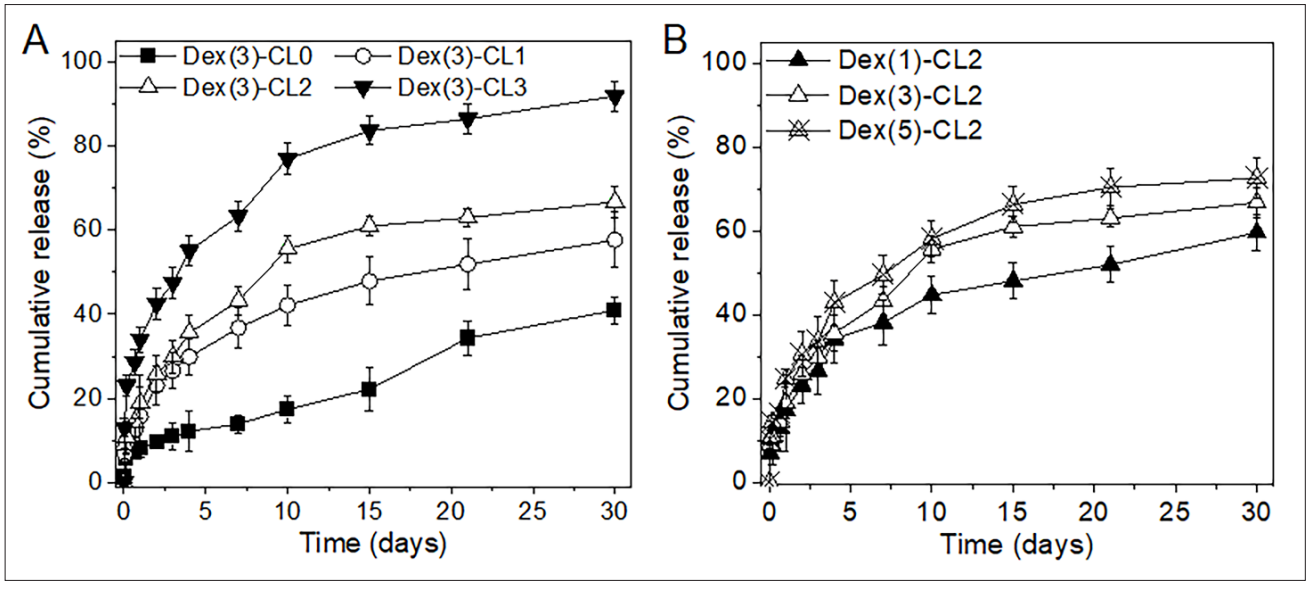


**Figure 7.** *In vitro* cumulative release profiles of Dex from Dex-CL depots over a 30-day period. (A) Dex release profiles from Dex-CL depots formulated with different polymer inks: CL0, CL1, CL2, and CL3. (B) Dex release profiles from Dex-CL2 depots with varying Dex concentrations (1, 3, and 5 wt%). Note: Molar ratio of L-lactide to ε-caprolactone for CL0 = $C_{100}L_0$, CL1 = $C_{99}L_1$, CL2 = $C_{91}L_9$, and CL3 = $C_{85}L_{15}$. Abbreviations: CL, poly(ε-caprolactone-ran-lactide); Dex, dexamethasone; Dex-CL, dexamethasone-loaded CL.

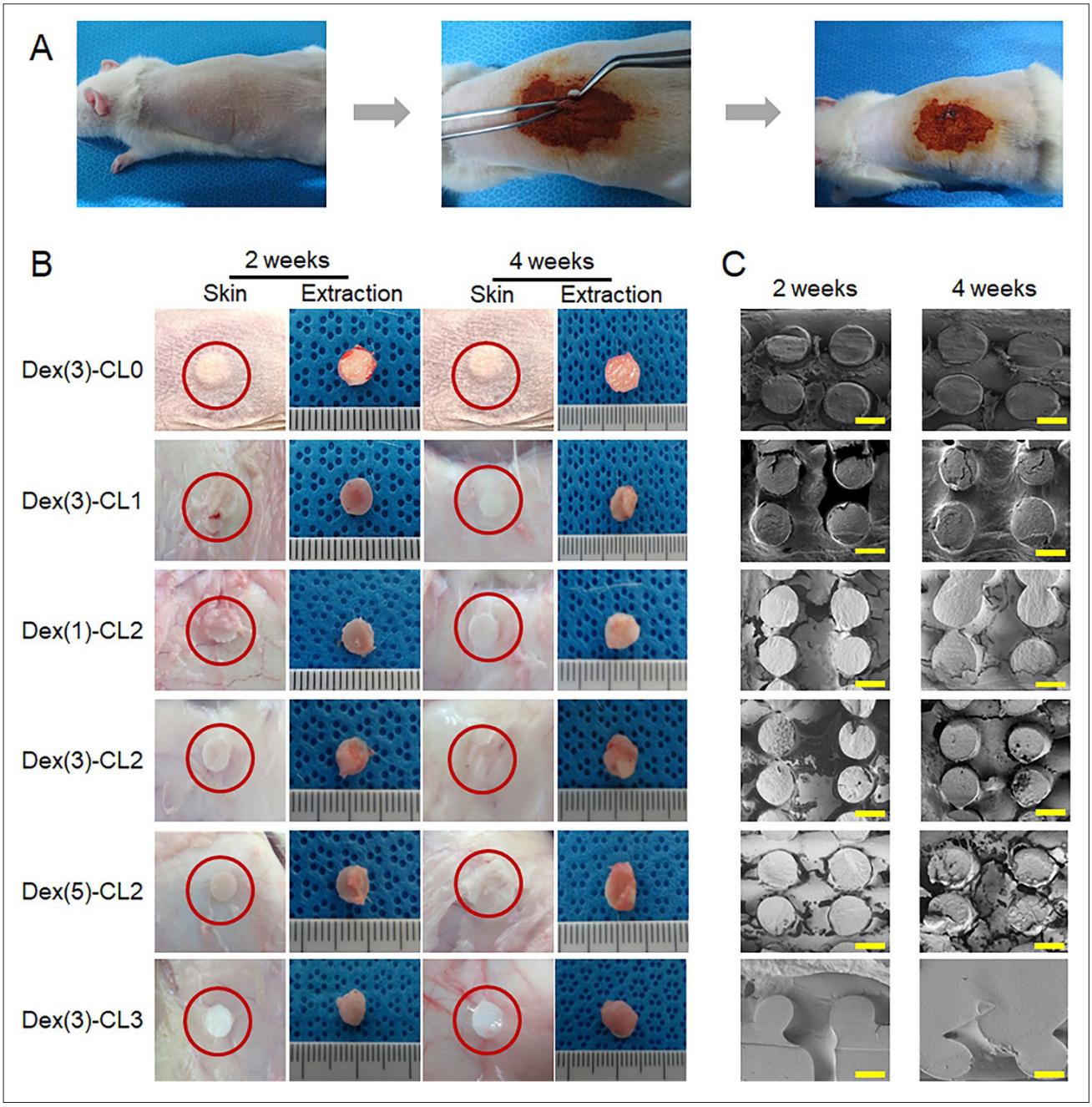


**Figure 8.** *In vivo* implantation of printed Dex-CL depots. (a) Subcutaneous implantation of Dex-CL depots in Sprague–Dawley rats. (b) Photographs and (c) scanning electron microscopy images (scale bar = 100 μm; magnification = 100×) of the Dex-CL depots on the skin and of the explanted Dex-CL depots at 2 and 4 weeks post-implantation. Abbreviations: CL, poly(ε-caprolactone-ran-lactide); Dex, dexamethasone; Dex-CL, dexamethasone-loaded CL.

respectively. The higher initial release from Dex-CL3 likely reflects enhanced surface diffusion and matrix softening at body temperature, improving drug accessibility at the depot–tissue interface. Although polymer melting alone does not fully account for the burst release, thermally induced matrix swelling appears to accelerate drug diffusion from the outer layers.

Following the initial phase, Dex was steadily released over the subsequent 3 weeks, consistent with a diffusion-dominated mechanism. For Dex-CL2 depots, higher Dex loading concentrations produced proportionally greater initial release, while long-term release rates remained relatively consistent, suggesting that drug loading affects

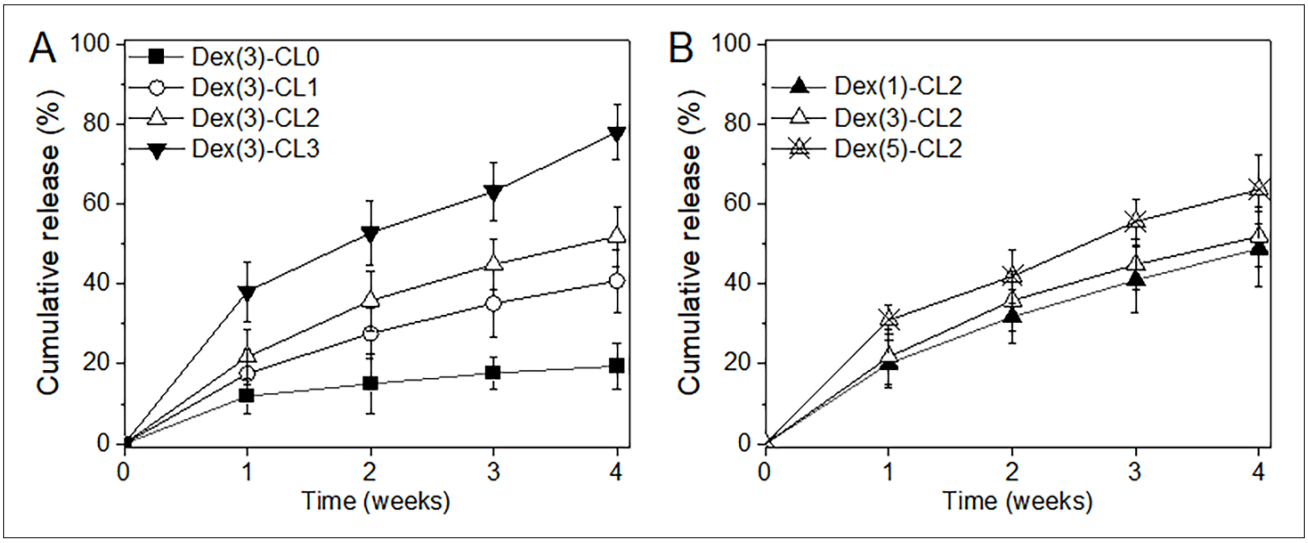


**Figure 9.** *In vivo* cumulative release of Dex from Dex-CL depots over 4 weeks. (A) Dex release profiles from Dex-CL depots formulated with different polymer inks: CL0, CL1, CL2, and CL3. (b) Dex release profiles from Dex-CL2 depots with varying Dex concentrations. Note: Molar ratio of L-lactide to ε-caprolactone for CL0 = $C_{100}L_0$, CL1 = $C_{99}L_1$, CL2 = $C_{91}L_9$, and CL3 = $C_{85}L_{15}$. Abbreviations: CL, poly(ε-caprolactone-ran-lactide); Dex: dexamethasone; Dex-CL, dexamethasone-loaded CL.

the magnitude of burst release without substantially altering sustained release behavior.

The *in vivo* drug release evaluation of the Dex-CL depots demonstrated that controlled release can be achieved by tuning the $T_m$ of the polymer over the 4-week implantation period. Rheological analysis confirmed that polymers with $T_m$ values closer to body temperature exhibited enhanced chain mobility, supporting the design rationale of this study. However, direct *in vivo* validation of thermal responsiveness was not performed in this work, and future studies will investigate the effects of carrier $T_m$ and other thermal property changes on drug release behavior.

### 3.10. *In vivo* host response to 3D-printed Dex-CL depots

Biocompatibility and immunomodulatory effects were assessed by subcutaneously implanting the 3D-printed Dex(1)-CL2, Dex(3)-CL2, Dex(5)-CL2, and Dex-CL3 depots in rats. Histological evaluations were performed at 2 and 4 weeks post-implantation using H&E staining and ED1 immunostaining to examine local tissue response and macrophage infiltration.

Histological analysis confirmed that all depot types generally maintained their structural integrity, with host tissue and neovasculature encapsulating the implants. H&E staining showed evidence of new tissue formation in all groups, with only minor histological differences among the depot types (Figure 10A). Notably, Dex-CL depots exhibited enhanced tissue remodeling compared to their Dex-free counterparts, suggesting that sustained Dex release modulated the local tissue microenvironment to support integration.

Among the tested formulations, Dex-CL3 exhibited partial dissolution *in vivo* due to its low $T_m$ (~40°C), leading to accelerated Dex release and deeper tissue infiltration. This was accompanied by a noticeable reduction in inflammatory cell infiltration. However, the thermal softening of Dex-CL3 also contributed to structural collapse, which may limit long-term mechanical stability.

To further evaluate the immune response, ED1 immunostaining was used to detect macrophage infiltration (Figure 10B). ED1-positive cells (red) and DAPI-stained nuclei (blue) were observed along the depot surface and in surrounding tissues across all groups. Quantitative analysis (Figure 10C) revealed that Dex-CL depots induced significantly lower macrophage infiltration. In all groups, macrophage counts peaked at 2 weeks and decreased by Week 4, consistent with the resolution phase of acute inflammation.

Importantly, Dex-CL depots demonstrated a more pronounced decline in ED1-positive cell counts over time, indicating that sustained Dex release effectively attenuated the host immune response. These results highlight the dual functionality of Dex-CL depots in providing both structural support and localized immunomodulation. By fine-tuning Dex release kinetics alongside thermal and mechanical properties, 3D-printed Dex-CL depots present

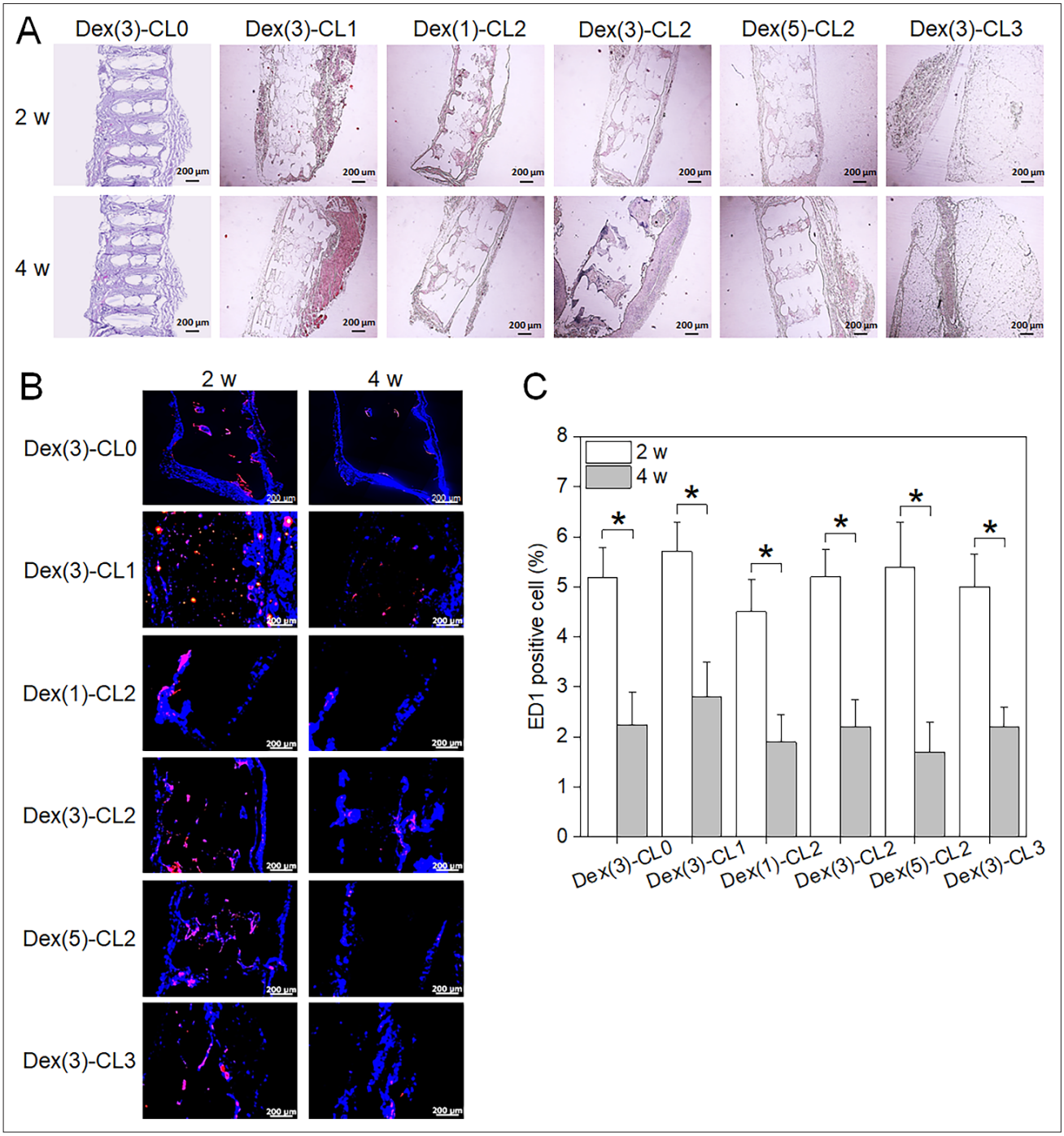


**Figure 10.** Hematoxylin and eosin (H&E) staining and immunofluorescence ED1 staining of Dex-CL depots explanted at 2 and 4 weeks post-implantation. Representative histological images showing tissue morphological changes over the implantation period: (A) H&E staining, (B) ED1 staining, and (C) quantification of ED1-positive area to assess inflammatory cell infiltration (magnification: 100×; scale bar: 200 μm). Data represent inflammatory ED1 expression. Note: $^*p < 0.05$. Abbreviation: Dex-CL, dexamethasone-loaded CL.

strong potential as subcutaneously implantable drug delivery platforms for long-term therapeutic applications.

## 4. Discussion

This study investigated the feasibility of using CL copolymer inks as thermally tunable matrices for fabricating implantable drug delivery depots via FDM. Unlike PLA, a commonly used FDM filament that requires high processing temperatures,[22] CL copolymers exhibit controllable melting transitions within a clinically relevant range of 40–60°C. This tunability enables the rational design of depots with controlled degradation and tailored release kinetics, addressing critical needs in localized and personalized drug delivery.[23–27]

Among available printing methods, FDM offers reproducibility, geometric fidelity, and structural stability without the need for solvents or crosslinking. In contrast, semi-solid extrusion allows lower-temperature processing but often requires solvent evaporation or chemical curing, which can limit precision and introduce cytotoxic residues. In this work, CL copolymer inks for FDM were designed to provide a balanced approach, yielding reliable microarchitecture, interconnected porosity, and mechanical robustness suitable for long-term implantation. Furthermore, rheological analysis confirmed that printability was strongly governed by the $T_m$ and viscoelastic properties of the copolymer formulations.

A key consideration in this study was the effect of copolymer composition on microstructural fidelity. High-fidelity depots produced with CL0–CL2 maintained the designed geometry within ±10% accuracy, demonstrating the suitability of these copolymers as reliable printing inks. By contrast, CL3 and, in particular, CL4 exhibited pore collapse and excessive line widening, resulting in reduced structural fidelity. These findings suggest that while dimensional accuracy can be partially optimized through printing conditions, variations in copolymer composition—and the resulting physicochemical differences—play a decisive role in determining the structural fidelity of printed depots.

Beyond microstructural considerations, *in vivo* evaluations of Dex-CL depots confirmed stable and sustained release of Dex over a 4-week period. However, depots fabricated from CL copolymer inks with $T_m$ relatively close to body temperature exhibited greater softening under physiological conditions, leading to accelerated release and reduced predictability. These results imply that melting transitions near physiological temperatures can influence release kinetics by enhancing copolymer chain mobility and swelling.

The substrate platform was maintained at ambient laboratory temperature (23–25°C) without active cooling, while only the enclosed printing chamber surrounding the extrusion nozzle was heated to the designated range of 80–120°C. This configuration ensured that the deposited filaments rapidly solidified upon contact with the cooler substrate, thereby preserving structural fidelity. Notably, chamber temperatures up to 100°C (the optimal printing condition) were substantially lower than the $T_m$ of pure PLA (>160°C), underscoring the rationale for employing CL copolymer inks designed to achieve melt processability at reduced temperatures. The upper limit of 120°C was investigated solely to assess comparative processability and was not used for final DDS fabrication. Importantly, the short residence time of the CL copolymer inks in the heated chamber (3–5 min per unit, maximum 25 min for multi-unit runs) further minimized the risk of drug degradation.

Within this context, Dex was selected as the model drug due to its well-documented thermal stability up to ~200°C,[21] making it highly compatible with the FDM process at ~100°C. However, such conditions may not be appropriate for thermolabile drugs. To address this limitation, CL copolymer ink design strategies—such as adjusting the CL content—can be employed to lower the melting transition and enable printing below 100°C. Through careful compositional tuning, it is anticipated that depots containing moderately heat-sensitive drugs can be fabricated under optimized conditions while preserving drug stability. Although this approach may not extend to highly unstable proteins or peptides, which generally cannot withstand even slight elevations above body temperature, it remains well-suited for a wide range of small-molecule therapeutics, including corticosteroids, anti-inflammatory agents, and thermally stable antibiotics. Future studies will systematically explore these drug classes to broaden the clinical applicability of this platform.

Regarding biocompatibility, the present short-term implantation studies (4 weeks) revealed no significant inflammation or tissue damage, suggesting the safety of Dex-CL depots. Nevertheless, it should be noted that lactide degradation can generate acidic byproducts, which may influence local tissue responses over longer implantation periods.[28] Comprehensive long-term studies will therefore be required to fully establish clinical safety and confirm compatibility for chronic use.

## 5. Conclusion

This work establishes CL copolymers as versatile polymer inks for FDM-based implantable DDS. By integrating tunable composition, structural fidelity, and degradation behavior, the system enables controlled release of stable

small molecules over clinically relevant timescales. Limitations include the need for direct validation of thermal responsiveness and extension to more thermolabile drugs. Even so, the rational design framework presented here provides a promising foundation for developing 3D-printed depots with customizable release profiles, potentially advancing treatments for chronic inflammation, localized cancer therapy, and other conditions requiring sustained drug delivery. Furthermore, our ongoing studies are exploring advanced implant depot designs incorporating psychotropic drugs and distinct CL copolymer inks. These constructs are intended to enable spatially controlled, sequential drug release, thereby expanding the versatility of CL-based FDM systems.

## Acknowledgments

None.

## Funding

This study was supported by grants from the National Research Foundation of Korea (NRF), the Science, Technology, Engineering, Arts, and Mathematics (STEAM) Program (RS-2024-00458419), and the Ministry of Small & Medium-sized Enterprises and Startups (20224371).

## Conflict of interest

Moon Suk Kim serves as an Editorial Board Member of the journal but was not involved in the editorial or peer-review process for this manuscript, either directly or indirectly. The other authors declare no competing interests.

## Author contributions

*Conceptualization:* Moon Suk Kim, Yun Geun Jeong, Joon Yeong Park, Sang Jin Lee, James J. Yoo
*Formal analysis:* Moon Suk Kim, Yun Geun Jeong
*Investigation:* Yun Geun Jeong, Joon Yeong Park, Moon Hee Lim
*Methodology:* Moon Suk Kim, Yun Geun Jeong, Joon Yeong Park, Sang Jin Lee, James J. Yoo
*Writing–original draft:* Yun Geun Jeong, Moon Suk Kim
*Writing–review & editing:* Moon Suk Kim

## Ethics approval and consent to participate

All animal experiments were approved by the Institutional Animal Care and Use Committee of Ajou University School of Medicine (Approval No. 2024-0030) and conducted in accordance with institutional ethical guidelines. Six-week-old male Sprague–Dawley (SD) rats (280–300 g) were used to evaluate the *in vivo* biocompatibility and drug release behavior of CL and Dex-CL depots. No experiments involving human subjects were conducted in this study.

## Consent for publication

Not applicable.

## Availability of data

Data are available from the corresponding author upon reasonable request.

## Further disclosure

Part or all of the findings have been presented at the following academic conferences:

1. Poster presentation: Yungeun Jeong (presenter), Joon Yeong Park (co-author), and Moon Suk Kim (corresponding author) at The 12th World Biomaterials Congress (WBC 2024), held from May 26 to 31, 2024, at EXCO, Daegu, Republic of Korea.
2. Poster presentation: Yungeun Jeong (presenter), Joon Yeong Park (co-author), and Moon Suk Kim (corresponding author) at The 2024 KSBM Fall Meeting & Tutorial Symposium, held from November 21 to 23, 2024, at SONO Belle JEJU, Jeju, Republic of Korea.
3. Poster presentation: Yungeun Jeong (presenter), Joon Yeong Park (co-author), and Moon Suk Kim (corresponding author) at The 25th Annual Conference of the Korean Tissue Engineering and Regenerative Medicine Society (KTERMS 2025), held from May 2 to 3, 2025, at CHA Bio Complex, Seongnam, Republic of Korea.
4. Poster presentation: Yungeun Jeong (presenter), Joon Yeong Park (co-author), and Moon Suk Kim (corresponding author) at The 36th International Symposium on Polymer Analysis and Characterization (ISPAC 2025), held from June 23 to 27, 2025, at Nanyang Technological University, Singapore.
5. Poster presentation: Joon Yeong Park (presenter) and Moon Suk Kim (corresponding author) at the 6th World Congress of the Tissue Engineering and Regenerative Medicine International Society (TERMIS2021) (Note: some of the printing-related data were submitted to the World Congress, but the presentation did not take place due to the COVID-19 pandemic in 2021.)

## References


1. Sadia M, Arafat B, Ahmed W, Forbes RT, Alhnan MA, 2018, Channelled tablets: An innovative approach to accelerating drug release from 3D printed tablets. *J Control Release*, 269:355–363.
doi: 10.1016/j.jconrel.2017.11.022

2. Melocchi A, Uboldi M, Maroni A, Foppoli A, Palugan L, Zema L, Gazzaniga A, 2020, 3D printing by fused deposition modeling of single- and multi-compartment hollow systems for oral delivery: A review. *Int J Pharm*, 579:119155.
doi: 10.1016/j.ijpharm.2020.119155

3. Yuan X, Wang Z, Che L, Lv X, Xu J, Shan S, Guo B, 2024, Recent developments and challenges of 3D bioprinting technologies. *Int J Bioprinting*, 10(2):1752.
doi: 10.36922/ijb.1752

4. Jeong YG, Yoo JJ, Lee SJ, Kim MS, 2024, 3D digital light process bioprinting: Cutting-edge platforms for resolution of organ fabrication. *Mater Today Bio*, 26:101284.
doi: 10.1016/j.mtbio.2024.101284

5. Ivorra-Martinez J, Ferrer I, Aguado R, Delgado-Aguilar M, Garcia-Romeu ML, Boronat T, 2024, Development of P(3HB-co-3HHx) nanohydroxyapatite (nHA) composites for scaffolds manufacturing by means of fused deposition modeling. *Int J Bioprinting*, 10(1):0156.
doi: 10.36922/ijb.0156

6. Ji YB, Park JY, Kang Y, Lee S, Ju HJ, Choi S, Lee BY, Kim MS, 2021, Scaffold printing using biodegradable poly(1,4-butylene carbonate) ink: Printability, *in vivo* physicochemical properties, and biocompatibility. *Mater Today Bio*, 12:100129.
doi: 10.1016/j.mtbio.2021.100129

7. Kwon DY, Park JY, Lee BY, Kim MS, 2020, Comparison of scaffolds fabricated via 3D printing and salt leaching: *In vivo* imaging, biodegradation, and inflammation. *Polymers*, 12(10):2210.
doi: 10.3390/polym12102210

8. Hou Y, Liu X, Wang X, Ji S, Gu Q, 2024, The application of 3D bioprinting technology in liver manufacturing: Progress, challenges, and prospects. *Int J Bioprinting*, 10(5):3819.
doi: 10.36922/ijb.3819

9. Balla E, Daniilidis V, Karlioti G, Kalamas T, Stefanidou M, Bikiaris ND, Vlachopoulos A, Koumentakou I, Bikiaris DN, 2021, Poly(lactic acid): A versatile biobased polymer for the future with multifunctional properties—From monomer synthesis, polymerization techniques and molecular weight increase to PLA applications. *Polymers*, 13(11):1822.
doi: 10.3390/polym13111822

10. Park JH, Park SH, Park JY, Ju HJ, Ji YB, Kim JH, Min BH, Kim MS, 2020, Preparation and characterization of biodegradable and hemocompatible copolymers. *React Funct Polym*, 146:104373.
doi: 10.1016/j.reactfunctpolym.2019.104373

11. Park JH, Lee BK, Park SH, Kim MG, Lee JW, Lee HY, Lee HB, Kim JH, Kim MS, 2017, Preparation of biodegradable and elastic poly(ε-caprolactone-co-lactide) copolymers and evaluation as a localized and sustained drug delivery carrier. *Int J Mol Sci*, 18(3):671.
doi: 10.3390/ijms18030671

12. Park JY, Park SH, Ju HJ, Ji YB, Yun HW, Min BH, Kim MS, 2020, Preparation of a cross-linked cartilage acellular matrix-poly(caprolactone-ran-lactide-ran-glycolide) film and testing its feasibility as an anti-adhesive film. *Mater Sci Eng C*, 117:111283.
doi: 10.1016/j.msec.2020.111283

13. Shi Y, Wang L, Sun L, Qiu Z, Qu X, Dang J, Zhang Z, He J, Fan H, 2023, Melt electrospinning writing PCL scaffolds after alkaline modification with outstanding cytocompatibility and osteoinduction. *Int J Bioprinting*, 9(6):1071.
doi: 10.36922/ijb.1071

14. Slavković V, Hanželič B, Plesec V, Milenković S, Harih G, 2024, Thermo mechanical behavior and strain rate sensitivity of 3D printed polylactic acid (PLA) below glass transition temperature. *Polymers*, 16(11):1526.
doi: 10.3390/polym16111526

15. Chen XB, Anvari-Yazdi AF, Duan X, Zimmerling A, Gharraei R, Sharma NK, Sweilem S, Ning L, 2023, Biomaterials / polymer inks and extrusion bioprinting. *Bioact Mater*, 28:511–536.
doi: 10.1016/j.bioactmat.2023.06.006

16. Hyun H, Kim MS, Jeong SC, Kim YH, Lee SY, Lee HB, Khang G, 2006, Preparation of diblock copolymers consisting of methoxy poly(ethylene glycol) and poly(ε-caprolactone)/poly(L-lactide) and their degradation property. *Polym Eng Sci*, 46(7): 1004–1011.
doi: 10.1002/pen.20581

17. Xu F, Rui S, Yang C, Jiang X, Wu W, Tang X, Armstrong DG, Ma Y, Deng W, 2023, Bioprinting technology for the management of diabetic foot disease: Emerging applications, challenges, and prospects. *Int J Bioprinting*, 9(6):0142.
doi: 10.36922/ijb.0142

18. Popescu D, Stochioiu C, Baciu F, Iacob MC, 2023, 3D-printed polycaprolactone mechanical characterization and suitability assessment for producing wrist–hand orthoses. *Polymers*, 15(3):576.
doi: 10.3390/polym15030576

19. Park HS, Park JH, Oh M, Yu K, 2024, Advancements in 3D bioprinting for precision medicine: Enhancing patient-derived organoids and extracellular vesicle applications in inflammatory diseases. *Int J Bioprinting*, 10(5):4054.
doi: 10.36922/ijb.4054

20. Rahul VG, Wilson J, Thomas LV, Nair PD, 2022, Assessing the 3D printability of an elastomeric poly(caprolactone-co-lactide) copolymer as a potential material for 3D printing tracheal scaffolds. *ACS Omega*, 7(8):7006–7016.
doi: 10.1021/acsomega.1c06679

21. Domsta V, Boralewski T, Ulbricht M, Schick P, Krause J, Seidlitz A, 2024, Stability of dexamethasone during hot-melt extrusion of filaments based on Eudragit® RS, ethyl cellulose and polyethylene oxide. *Int J Pharm*, 8:100263.
doi: 10.1016/j.ijpx.2024.100263

22. Mazur J, Sobczak P, Panasiewicz M, et al., 2025, Mechanical properties and biodegradability of samples obtained by 3D printing using FDM technology from PLA filament with by-products. *Sci Rep*, 15:5847.
doi: 10.1038/s41598-025-89984-0

23. Botlhoko OJ, Ramontja J, Ray SS, 2018, A new insight into morphological, thermal, and mechanical properties of melt-processed polylactide/poly(ε-caprolactone) blends. *Polym Degrad Stab*, 154:84–95.
doi: 10.1016/j.polymdegradstab.2018.05.025

24. Navarro-Baena I, Sessini V, Dominici F, Torre L, Kenny JM, Peponi L, 2016, Design of biodegradable blends based on PLA and PCL: From morphological, thermal and mechanical studies to shape memory behavior. *Polym Degrad Stab*, 132:97–108.
doi: 10.1016/j.polymdegradstab.2016.03.037

25. Urquijo J, Guerrica-Echevarría G, Eguiazábal JI, 2015, Melt processed PLA/PCL blends: Effect of processing method on phase structure, morphology, and mechanical properties. *J Appl Polym Sci*, 132(29):42641.
doi: 10.1002/app.42641

26. Gao H, Li J, Li Z, Li Y, Wang X, Jiang J, Li Q, 2023, Enhancing interfacial interaction of immiscible PCL/PLA blends by in-situ crosslinking to improve the foamability. *Polym Test*, 124:108063.
doi: 10.1016/j.polymertesting.2023.108063

27. Cerveto T, Denis L, Stoops M, Lechanteur A, Choisnard L, 2024, The promising role of semi-solid extrusion technology in custom drug formulation for pediatric medicine. *Int J Bioprinting*, 10(6):4063.
doi: 10.18063/ijb.v10i6.4063

28. Wang X, Liu D, 2024, Macrophage polarization: A novel target and strategy for pathological scarring. *Tissue Eng Regen Med*, 21:1109–1124.
doi: 10.1007/s13770-024-00509-7